[Geophysical Research Letters]

Supporting Information for

[Heat flux distribution of Antarctica unveiled]

[Y. M. Martos[1,2,3], M. Catalan[4], T. A. Jordan[1], A. Golynsky[5], D. Golynsky[5], G. Eagles[6], D. G. Vaughan[1]]

[1British Antarctic Survey (NERC), High Cross, Madingley Rd, Cambridge CB3 0ET, United Kingdom.

2Now at the University of Maryland College Park, Department of Astronomy, College Park, MD 20742, United States of America.

3Now at NASA Goddard Space Flight Center, Planetary Magnetospheres Laboratory, 8800 Greenbelt Rd, Greenbelt, MD 20771, United States of America.

4Royal Observatory of the Spanish Navy, c/ Cecilio Pujazón, s/n, 11100 San Fernando, Cádiz, Spain.

5The All-Russia Scientific Research Institute for Geology and Mineral Resources of the Ocean, 1, Angliysky Avenue, Saint-Petersburg, 190121, Russia.

6Alfred Wegener Institute for Polar and Marine Research, Am Alten Hafen 26, Bremerhaven, 27568, Germany.

Corresponding author: Yasmina M. Martos (yasmina.martos@nasa.gov)]

Contents of this file

Introduction

[This Supplementary Information file includes the detailed description of the spectral method for determining the Curie Depth, figures related to the spectrum methodology and the geothermal heat flux uncertainty. All maps are in polar stereographic projection. Additionally, a table compiling the magnetic surveys/compilations used to create the Antarctic magnetic anomaly map and a table compiling the available local geothermal heat flux values derived by direct measurements, temperature profiles and more indirect methodologies are presented. A

table with the statistical analysis between the local values and the different heat flux maps is also included.

Curie Depth estimate method

Magnetic anomalies are sensitive to the thermal profile of the lithosphere. We derived Curie Depth estimates from the magnetic anomaly map by using spectral methods. There are different methods to estimate the base of the magnetic sources [*Ravat et al.*, 2007] and based on a critical evaluation of several different spectral magnetic depth determination techniques, we selected the de-fractal spectral method as it is appropriate for regional compilations of magnetic anomalies and it has been extensively used to estimate the Curie Depth [*Bouligand et al.*, 2009; *Salem et al.*, 2014; *Khojamli et al.*, 2017]. Figure S1 shows the flowchart of the procedure we followed.

The de-fractal spectral method does not assume a random and uncorrelated distribution of sources, but follows a fractal/scale distribution [*Maus and Dimri*, 1995; *Bansal et al.*, 2011]. This considers that there is a relationship between the observed power spectral density and the power spectral density of the random magnetization model (1):

$$P_R(k_x, k_y) = P_F(k_x, k_y) \cdot k^{\alpha} \qquad (1)$$

where $P_F(k_x, k_y)$ is the observed power spectrum, $P_R(k_x, k_y)$ represents the power spectrum due to random magnetization modeling, k is referred to radial wavenumber, and α denotes the fractal parameter. The fractal parameter, α, is related to the fractal parameter of magnetization, β, by α = β - 1.

If the fractal parameter is known, once the fractal effect of the magnetization spectrum is removed we estimated the depth to the top, Z_t, and depth to the centroid, Z_o, of the magnetic sources following the procedure of *Tanaka et al.* [1999], which is known as the centroid spectral method. This method is appropriate for regional compilations of magnetic anomalies and has been extensively used to estimate the Curie Depth in other regions [*Tanaka et al.*, 1999; *Ravat et al.*, 2007; *Bouligand et al.*, 2009; *Li et al.*, 2009, 2010, 2011; *Salem et al.*, 2014; *Vargas et al.*, 2015; *Khojamli et al.*, 2017; *Salazar et al.*, 2017]. To infer the Curie Depth we follow these steps:

- First we estimate the depth to the top of the deepest magnetic body, Z_t. For this we used the relationship between Z_t and the power spectrum due to random magnetization modeling, $P_R(k_x, k_y)$ (2). The simplified form, valid for wavelengths less than about twice the thickness of the layer, is [*Spector and Grant*, 1970]:

$$ln\left(P_R(|k|)^{1/2}\right) = A - |k|Z_t \quad (2)$$

where *A* is a constant and *k* is the wavenumber. The depth to the top is estimated from (2) by fitting a straight line through the high wavenumber part of the radially average spectrum of $ln\left(P_R(|k|)^{1/2}\right)$ (Figure S2a).

- Second we estimate the depth of the centroid of the deepest magnetic body, Z_o. For this we used the relationship between Z_o and the power density spectrum (3), which is a good approximation at low wavenumbers:

$$ln\left(P_R(|k|)^{1/2}\Big/_{|k|}\right) = \ln(D) - |k|Z_o \quad (3)$$

where D is a constant. The depth to the centroid estimate is calculated using (3) by fitting a straight line through the low wavenumber parts of the radially average spectrum of $ln\left(P_R(|k|)^{1/2}\Big/_{|k|}\right)$ (Figure S2b).

- Finally the Curie Depth or depth to the bottom of the magnetic source, Z_b, is then inferred applying (4).

$$Z_b = 2Z_O - Z_t \quad (4)$$

To optimize the window dimensions we assessed the ability of each window size to identify the "peak" in the $ln\left(P_R(|k|)^{1/2}\right)$ spectrum (Figure S2a). East and West Antarctica were treated separately since they present different radial average power density spectra due to their differences in geology and evolution [*Dalziel and Elliot*, 1982]. The position of the peak depends on the size of the window selected for applying the spectral method, which should be at least 10 times the expected depth to the bottom of the magnetic source [*Ravat et al.*, 2007]. So, using windows of 350 x 350 km for Antarctica is appropriate based on the expected depth of the bottom of the magnetic source, derived by seismology [*An et al.*, 2015b] and gravity [*Block et al.*, 2009] studies. Then, in order to ensure the continuity of the solutions and give continuity to long wavelength sources we used overlap between windows of 57%, giving a total of 1299 for our study area.

Once we obtained the spectra of every window across East and West Antarctica separately we calculated the average density power spectrum for each region, one for East Antarctica and one for West Antarctica (Figure S3). After this and considering the position of the peak we selected the appropriate range of wavenumbers for calculating the linear fits for Z_t and Z_o in each region. The wavenumber ranges to calculate the Z_o were k =0.028-0.16 km^{-1} for East Antarctica and k =0.065-0.28 km^{-1} for West Antarctica. To estimate Z_t we selected a linear fit at high wavenumber ranges.

Accordingly, the ranges were k =0.26-0.40 km^{-1} for East Antarctica and k =0.32-0.48 km^{-1} for West Antarctica.

Commonly the fractal parameter, α, is not known. As the value of α is linked to the depth to the top as they are interdependent and strongly correlated [*Bouligand et al.*, 2009], there is no direct way but an iterative process to get it. For this reason, we checked different values for this parameter and selecting the best fit between the random magnetization model spectrum and the synthetic spectrum. This is defined as the theoretical spectrum derived after using the Z_t and Z_o calculated in the previous steps (5):

$$P_{syn}(|k|) = Ae^{-2|k|Z_t}\left(1 - e^{-|k|(Z_b - Z_t)}\right)^2 \quad (5)$$

After testing values of α ranging from 0 to 2 on 0.1 steps we obtained the best fit between the random magnetization model spectrum (eq. 1) and the synthetic spectrum (eq. 5) for α=0.2. Higher values of α provided an overcorrected spectrum.

The estimates Z_b are considered to be a representation of Curie Depth values for each window, and are geographically assigned to the center of every block. Depth uncertainties, ϵ, in Z_o and Z_t were always smaller than 15 % of the corresponding estimated depth [*Okubo and Matsunaga*, 1994] based on deviations between the spectrum and the straight line (eq. 6):

$$\epsilon = \frac{\sigma}{(k_u - k_l)} \quad (6)$$

where σ is the standard deviation of the differences between natural logarithm of the radially average power density spectrum and the linear fit by the least squares method. The denominator, $(k_u - k_l)$, is the range of wavenumbers used to estimate the linear relationship.

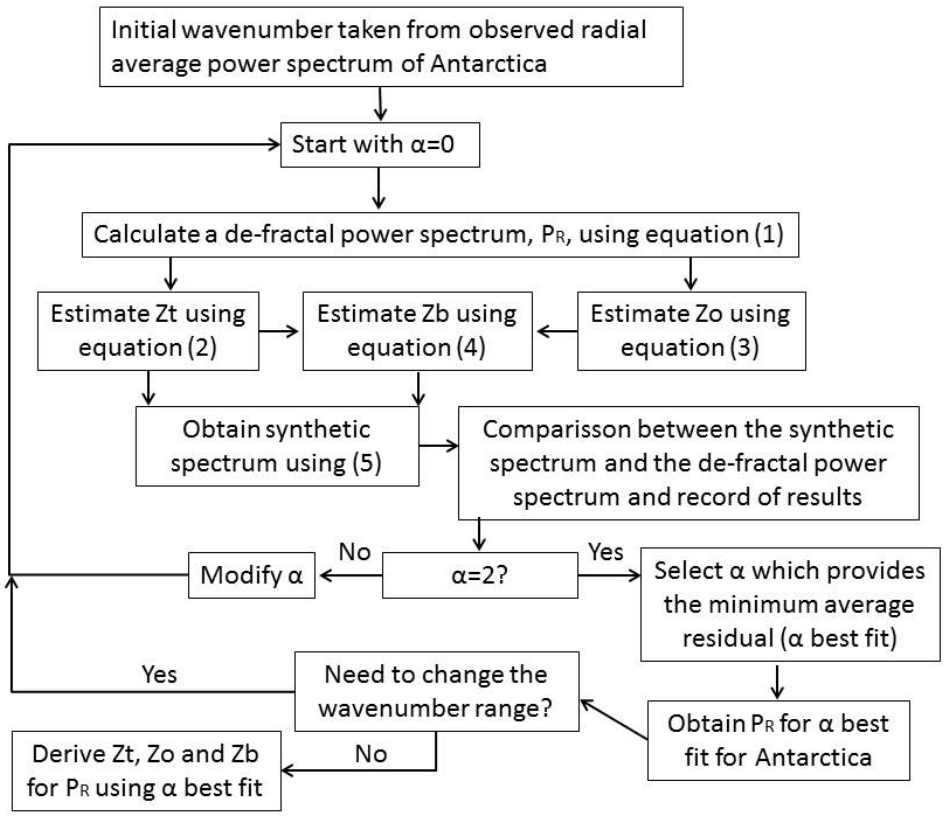

Figure S1. Flowchart diagram summarizing the procedure we used to estimate Curie Depths, Z_b.

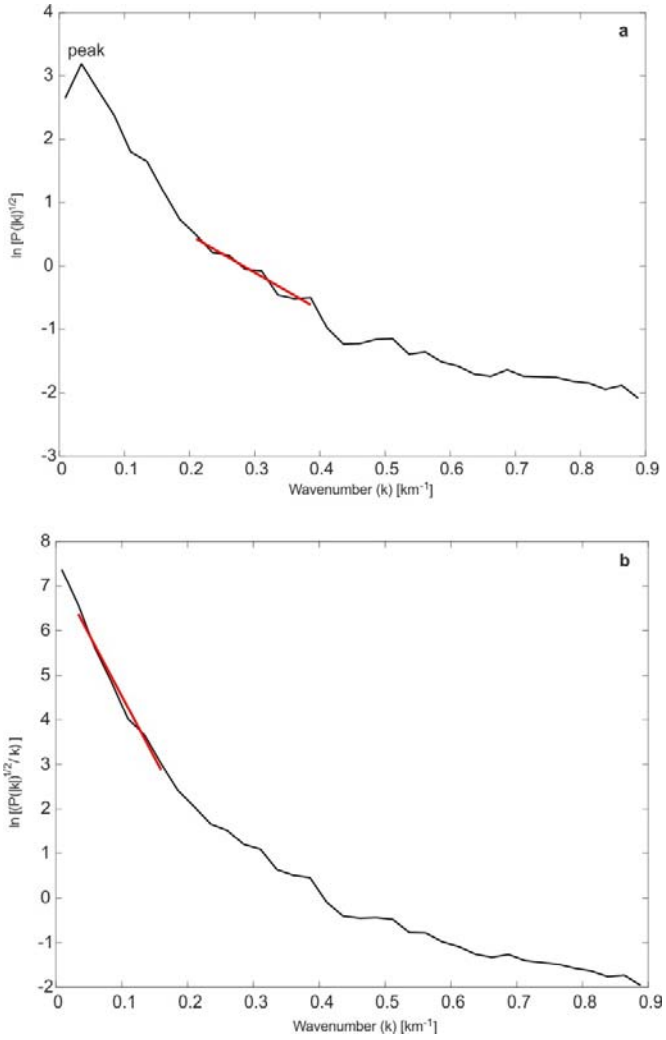

Figure S2. Example of spectra of a window. a) Calculation of the Zt from the radially average spectrum of $ln\left(P(|k|)^{1/2}\right)$. The peak is well identified in this case and it is marked in the figure. The range of wavenumbers selected is located in the high wavenumbers. The red line represents the fitting line we used to obtain Zt. b) Calculation of the Zo from the radially averaged spectrum of $ln\left(P(|k|)^{1/2}/_{|k|}\right)$. The range of wavenumbers selected is located in the low wavenumbers. The red line is the fitting line we used to obtain Zo.

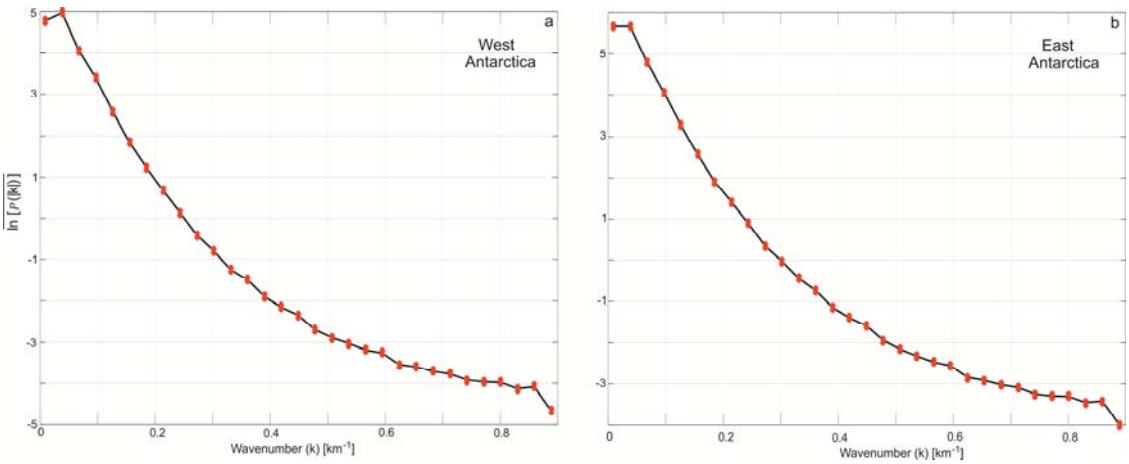

Figure S3. Average logarithmic power spectrum of all windows for West and East Antarctica separately.

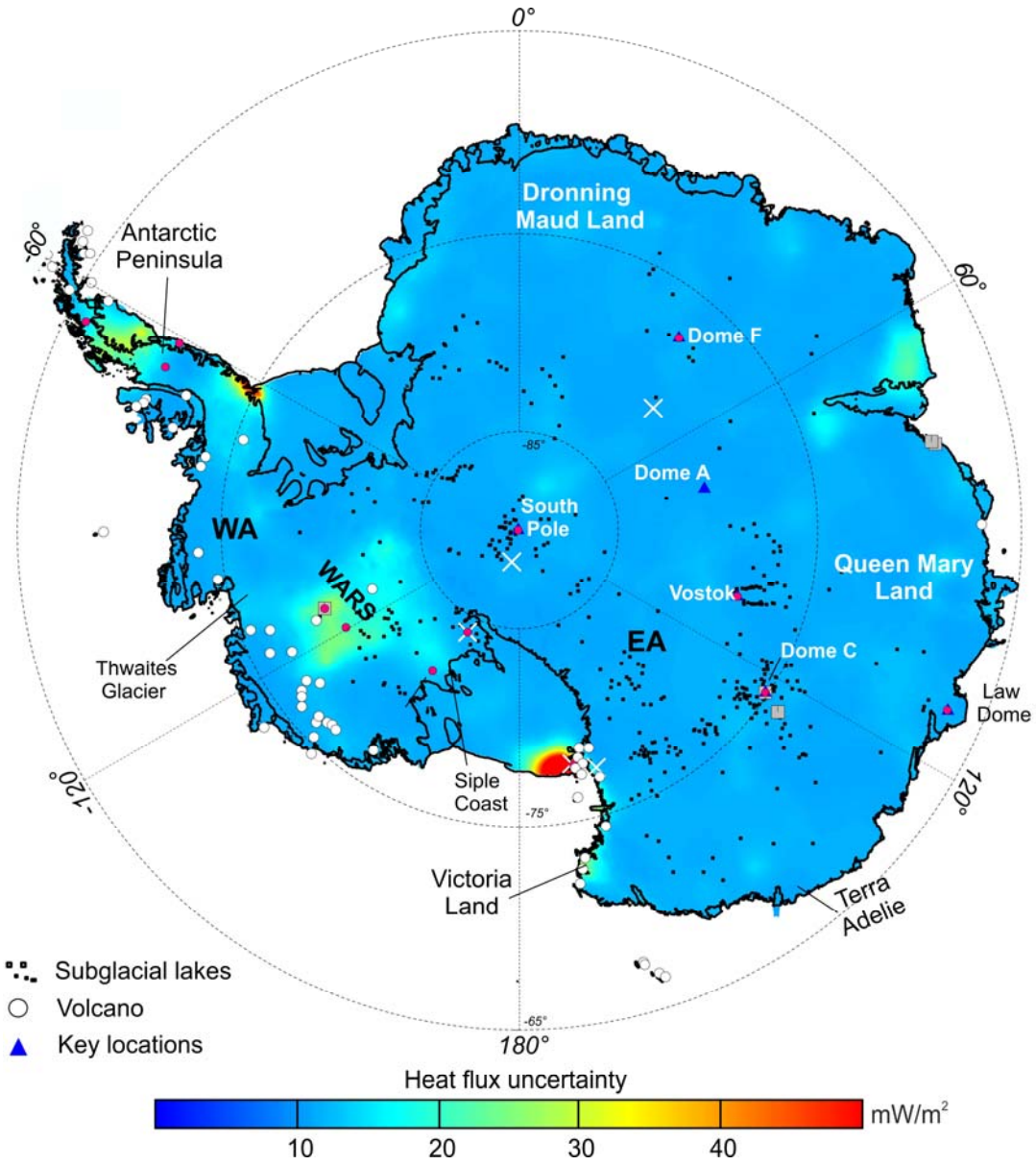

Figure S4. Heat flux uncertainty distribution calculated using the uncertainty propagation equation for independent errors. Volcanos [LeMasurier and Thomson, 1990], subglacial lakes [Wright and Siegert, 2012] and key locations are displayed.

Survey/compilation	Area covered	Type of data	Source	Reference
ADMAP	Part of the Antarctic continent and surrounding areas	5 km-resolution grid from compilation of international data	http://admap.kopri.re.kr/databases.html	*Golynsky et al.*, 2001
WISE	North of Wilkes Basin	Gridded 880m mesh raster, based on 8.8 km spaced line data from single survey.	British Antarctic Survey https://legacy.bas.ac.uk/data/aerogeo/access/wise-mag	*Ferraccioli et al.*, 2009
AFI-Coats Land	Coats Land	Gridded 4 km mesh raster, based on 40 km spaced line data from single survey.	British Antarctic Survey	*Bamber et al.*, 2006
AGAP	Gamburtsev Mountains	Gridded 500m mesh raster, based on 5 km spaced line data from single survey.	British Antarctic Survey	*Ferraccioli et al.*, 2011
PPT	Pensacola Pole Transect	Gridded 850m mesh raster, based on 10 km spaced line data from single survey.	Institute for Geophysics University of Texas at Austin	*Studinger et al.*, 2006
ICECAP	Aurora Basin region	2 km mesh raster	http://onlinelibrary.wiley.com/doi/10.1002/2014GL059405/full	*Aitken et al.*, 2014
Central TAM	Central Transantarctic Mountains	Gridded and point data Line spacing 1.25-2.5 km from single survey.	US Data Centers/US Antarctic Data Coordination Center	*Goodge and Finn, 2010*
Weddell Sea	Weddell Sea and surrounding areas	Gridded compilation with 2.5 km raster mesh.	British Antarctic Survey	*Jordan et al.*, 2017
Droning Maud Land	Droning Maud Land	Gridded compilation	Alfred Wegener Institute	*Mieth and Jokat*, 2014
ICEGRAV2013	Recovery Ice stream	Gridded 2 km mesh raster based on 27.5 km line spacing data from single survey.	British Antarctic Survey	*Forsberg et al.*, 2017
MF7	Satellite magnetic anomalies in Antarctica and surrounding areas	Gridded data at 5 km raster resolution	http://www.geomag.us/models/MF7.html	*Maus*, 2010

Table S1. Magnetic surveys/compilations used for creating the magnetic anomaly map of Antarctica and surrounding areas.

Site/Region	Longitude (°)	Latitude (°)	Heat flux (mW/m^2)	Heat flux error (mW/m^2)	Method	Reference	Comments
Bruce Plateau	-64.066666	-66.033333	85-88		Temperature profile	*Zagorodnov et al.* [2012]	Larissa Site beta
Byrd Station	-119.516666	-80.016666	75.3		Temperature profile	*Gow et al.* [1968]	
Concordia Trench	Dome C area		40	± 12	Modeled	*Carter et al.* [2009]	
Concordia Subglacial Lake (Shore)	125.05	-74.05	100		Modeled	*Carter et al.* [2009]	
Dolleman Island	-60.933333	-70.583333	100	± 5	Temperature profile	*Nicholls and Paren* [1993]	
Dome C Plateau	Dome C area		40	± 12	Modeled	*Carter et al.* [2009]	
Dome F	39.7	-75.1	59		Temperature profile	*Hondoh et al.* [2002]	
Dyer Plateau	-65.0	-70.5	100	± 5	Temperature profile	*Nicholls and Paren* [1993]	
EPICA Dome C	123.4	-75.1	66.8		Modeled	*Parrenin et al.* [2016]	Calculated using airborne radar and ice flow modeling
EPICA Dome C	123.4	-75.1	40-50		Temperature profile/Modeled	*Carter et al.* [2009], *Ritz et al.* [2010]	Evidence from the EPICA Dome C ice core

Hut Point Peninsula (Ross Island)	166.66805	-77.81888	164	± 60	Temperature profile	*Risk and Hochstein* [1974]	Short hole
Lake Vida	161.81	-77.38	85		Measurement	*Decker and Bucher* [1982]	
Lake Whillans	206.31	-84.24	285	± 80	Measurement	*Fisher et al.* [2015]	Measured in the base of the lake
Lake Whillans	206.31	-84.24	105	± 13	Temperature profile	*Fisher et al.* [2015]	Measured in the ice column
Law Dome	112.80	-66.76	75.1	± 0.6	Temperature profile	*Dahl-Jensen et al.* [1999]	
Lower Vincennes Basin	Dome C area		40	± 12	Modeled	*Carter et al.* [2009]	
McMurdo Ice Shelf	165.276765	-77.758141	81.5		Temperature profile	*Schröder et al.* [2011]	borehole AND-2A ANDRILL
McMurdo Ice Shelf	165.276765	-77.758141	115		Temperature profile	*Morin et al.* [2010]	borehole AND-1B ANDRILL
Nagursk-1	47.7083	-80.7788	57		Measurement	*Hasterok* [2010]	
Nagursk-1.2	-168.625	-88.375	54		Measurement	*Hasterok* [2010]	
Rauer Islands	77.83	-68.85	40		Modeled	*Carson et al.* [2014]	
Siple Coast Ice streams	Ross Sea Ice Shelf area in West Antarctica		80-100		Modeled	*Raymond* [2000]	Energy balance study
Siple Dome	-148.809	-81.658	69	± 1	Temperature profile	*Engelhardt* [2004]	
South Pole	0	-90	61		Temperature profile	*Price et al.* [2002]	
Southern Prydz Bay	Prydz Bay area		60-70		Modeled	*Carson et al.* [2014]	
Vostok	106.87	-78.45	50-56		Temperature	*Salamatin*	

					profile	*et al.* [1998], *Dmitriev et al.* [2016]	
Thwaites Glacier	West Antarctic Coast		114 (average)	± 10	Modeled	*Schröeder et al.* [2014]	Wide analysis of hydrology and basal reflectivity
Thwaites Glacier	West Antarctic Coast		97		Modeled	*Damiani et al.* [2014]	Geophysical analysis
Upper Vincennes Basin	Dome C area		60-70		Modeled	*Carter et al.* [2009]	
Vestfold Hills Block	78.25	-68.68	31		Modeled	*Carson et al.* [2014]	
West Antarctic Ice Sheet Divide Ice Core Site	-112.08562	-79.46765	240		Temperature profile	*Clow et al*. [2012]	Long hole

Table S2. Locations and heat flux values derived from different techniques in Antarctica. The values and locations have been considered as reference for our calculations. See Figure 3 for site locations in the map.

Heat Flux map	Mean value of differences (mW/m^2)	Standard deviation (mW/m^2)
This study	1.4	14.2
Shapiro and Ritzwoller [2004]	44.5	21.5
Fox Maule et al. [2005]	5.0	26.6
An et al. [2015]	0.8	28

Table S3. Mean value of differences between independence source for heat flux values and the different proposed maps, as well as their standard deviation.